Journal of Alloys and Compounds 502 (2010) L10–L13

Contents lists available at ScienceDirect

Journal of Alloys and Compounds

journal homepage: www.elsevier.com/locate/jallcom

Letter

Properties and densification of nanocrystalline $MoSi_2$–Si_3N_4 composite from mechanically alloyed powders by pulsed current-activated sintering

In-Young Ko [a], Hyun-Su Kang [a], Jung-Mann Doh [b], Jin-Kook Yoon [b], In-Jin Shon [a,c,*]

[a] Division of Advanced Materials Engineering, The Research Center of Advanced Materials Development, Chonbuk National University, 664-14 Deokjin-dong 1-ga, Deokjin-gu, Jeonju, Jeonbuk 561-756, Republic of Korea
[b] Advanced Functional Materials Research Center, Korea Institute of Science and Technology, PO Box 131, Cheongryang, Seoul 130-650, Republic of Korea
[c] Department of Hydrogen and Fuel Cells Engineering, Specialized Graduate School, Chonbuk National University, 664-14 Deokjin-dong 1-ga, Deokjin-gu, Jeonju, Jeonbuk 561-756, Republic of Korea

ARTICLE INFO

Article history:
Received 6 March 2010
Received in revised form 11 April 2010
Accepted 14 April 2010
Available online 24 April 2010

Keywords:
Powder metallurgy
Sintering
Nanostructured materials
Mechanical properties

ABSTRACT

Nanosized $MoSi_2$ and Si_3N_4 powders were synthesized from Mo_2N and Si powders by high-energy ball milling. A dense nanocrystalline $MoSi_2$–Si_3N_4 composite was consolidated using the pulsed current-activated sintering (PCAS) method within 3 min period from the mechanically activated $MoSi_2$ and Si_3N_4 powders. A highly dense $MoSi_2$–Si_3N_4 composite, with relative density of up to 97%, was produced under the simultaneous application of 80 MPa pressure and 2800 A pulsed current. The mean grain size, hardness, and fracture toughness of the composite were investigated.

1. Introduction

Transition-metal silicides have properties that make them quite attractive for high-temperature applications of up to 1300 °C or higher. These include a high melting point, high modulus, high oxidation resistance in air, and relatively low density [1,2]. Among the metal silicides, $MoSi_2$, in particular, has been examined regarding its potential material for both high-temperature structural applications and in the electronics industry. $MoSi_2$ provides a combination of several desirable properties, such as high melting point (2020 °C), high modulus (440 GPa), good oxidation resistance in air, relatively low density (6.24 g/cm^3) [3], and the ability to undergo plastic deformation above 1200 °C [4]. Combined with good thermal and electric conductivity, these properties have led to the use of $MoSi_2$ for heating elements in high-temperature furnaces operating in air up to approximately 1700 °C [5,6]. However, as with many intermetallic compounds, $MoSi_2$ exhibits low fracture toughness below the ductile–brittle transition temperature and low oxidation resistance [7–9]. One method for improving the mechanical properties and oxidation resistance is the addition of a second phase to form composites and nanostructured materials [10–14]. One example is the addition of Si_3N_4 to $MoSi_2$ to improve the latter's oxidation resistance [15]. At the same time, nanostructured materials have been widely investigated, since the comparatively large fraction of grain boundaries in such materials can yield unusual or improved mechanical, thermal, photocatalytic, magnetic, and biomedical properties [16–19]. Particularly, nanomaterials, in particular, have attracted more attention recently due to their high strength, high hardness, excellent ductility, and toughness [18,19]. It is well known that Si_3N_4 has a high thermal shock resistance due to its low thermal expansion coefficient, as well as good oxidation resistance compared to other structural materials [20,21]. The isothermal oxidation resistance of $NbSi_2$–40 vol.% Si_3N_4 composite prepared by spark plasma sintering (SPS) in dry air at 1300 °C is superior to that of a monolithic $NbSi_2$ compact [22]. Moreover, the low-temperature cyclic oxidation resistance of $MoSi_2$–Si_3N_4 nanocomposite coating formed on a Mo substrate in air at 500 °C is higher than that for monolithic $MoSi_2$ [15]. This effect is due to the larger amount of Si, which facilitates the formation of dense SiO_2 scale [15,22]. This suggests that Si_3N_4 may be the most promising additive for reinforcement of $MoSi_2$-based composites.

However, the grain size of sintered materials is much larger than that in pre-sintered powders, owing to the rapid grain growth that occurs during the conventional sintering processes. Controlling

* Corresponding author at: Division of Advanced Materials Engineering, The Research Center of Advanced Materials Development, Chonbuk National University, 664-14 Deokjin-dong 1-ga, Deokjin-gu, Jeonju, Jeonbuk 561-756, Republic of Korea. Tel.: +82 63 270 2381; fax: +82 63 270 2386.
E-mail address: ijshon@chonbuk.ac.kr (I.-J. Shon).

0925-8388/$ – see front matter © 2010 Elsevier B.V. All rights reserved.
doi:10.1016/j.jallcom.2010.04.120

grain growth during sintering is, therefore, a key to the commercial success of nanostructured materials. Recently, the pulsed current-activated sintering (PCAS) method, which can produce dense materials within 2 min, has been shown to be effective in achieving rapid densification to nearly the theoretical density while preventing grain growth in nanostructured materials [23,24].

In this regard, the present study investigated the preparation of nanosized $MoSi_2$ and Si_3N_4 powders from a mixture of Mo_2N and Si by high-energy ball milling and the consolidation of dense nanocrystalline $8MoSi_2$–Si_3N_4 composite fabricated by the PCAS method. The mechanical properties of the nanostructured $MoSi_2$–Si_3N_4 composite were evaluated.

2. Experimental procedures

The starting materials were Mo_2N (<1 μm, 99.993% pure, High purity chemicals laboratory) and Si (−325 mesh, 99.5% pure, Aldrich Products) powders. The required amounts of starting materials were mixed by a high-energy ball mill (Pulverisette-5 planetary mill) at 250 rpm for 20 h. Tungsten carbide balls (5 mm in diameter) were used as grinding media in a sealed cylindrical stainless steel vial under an argon atmosphere. A charge ratio (ratio of mass of balls to powder) of 30:1 was used. The grain size and internal strain were calculated from X-ray diffraction (XRD) data using the formula [25]

$$B_r(B_{crystalline} + B_{strain})\cos\theta = \frac{k\lambda}{L} + \eta\sin\theta \quad (1)$$

where B_r is the full width at half-maximum (FWHM) of the diffraction peak after an instrument correction; $B_{crystalline}$ and B_{strain} are the FWHM attributable to small grain size and internal stress, respectively; k is a constant (with a value of 0.9); λ is the wavelength of the X-ray radiation; L and η are the grain size and internal strain, respectively; and θ is the Bragg angle. The parameters B and B_r follow Cauchy's formula in the relationship $B = B_r + B_s$, where B and B_s are the FWHM of the broadened Bragg peaks and standard sample's Bragg peaks, respectively.

The ball-milled mixture was packed in a graphite die (with outside diameter 45 mm, inside diameter 20 mm, and height 40 mm) and placed into the PCAS system, as shown schematically in the literature [23,24]. The four major stages in the synthesis are as follows: evacuation of the system to 40 mTorr (stage 1), application of a uniaxial pressure of 80 MPa (stage 2), activation of a pulsed current of 2800 A, maintained until densification is achieved as indicated by a linear gauge measuring the level of sample shrinkage (stage 3), and cooling to room temperature (stage 4). The temperatures were measured using a pyrometer focused on the surface of the graphite die during the entire process. The relative density of the sintered sample was measured using the Archimedes· method. Prior to microstructure observation, the sintered samples were polished and etched for 1 min at room temperature using a solution composed of HF (15 vol.%), HNO_3 (35 vol.%) and H_2O (50 vol.%). The composition of the products was analyzed by XRD and the microstructure was examined by field emission scanning electron microscopy (FE-SEM) with energy dispersive X-ray analysis (EDAX). The Vickers hardness was measured by the indentations method with a load of 20 kg and a dwell time of 15 s.

3. Results and discussion

Fig. 1(c) shows XRD patterns from the high-energy ball-milled powders. The products, $MoSi_2$ and Si_3N_4 were detected but the Mo_2N, and Si reactant powders were not seen. A minor phase (Mo_5Si_3) was, however, observed. The presence of Mo_5Si_3 in the sample suggests a deficiency of Si. It is believed that this observation is due to entrapped oxygen in the pores of the interior portion of the sample, which may in turn be caused by the oxidation of Si during the ball milling process.

It can be concluded from the above result, that $8MoSi_2$–Si_3N_4 composite was synthesized from the Mo_2N and Si powders by the ball milling process. The interaction relating these phases, i.e.,

$$4Mo_2N + 19Si \rightarrow 8MoSi_2 + Si_3N_4, \quad (2)$$

is thermodynamically feasible.

Moreover, the high-energy ball milling resulted in a significant decrease in grain size of $MoSi_2$ and Si_3N_4. The average grain sizes of $MoSi_2$ and Si_3N_4, as measured using Eq. (1), were approximately 30 and 18 nm, respectively.

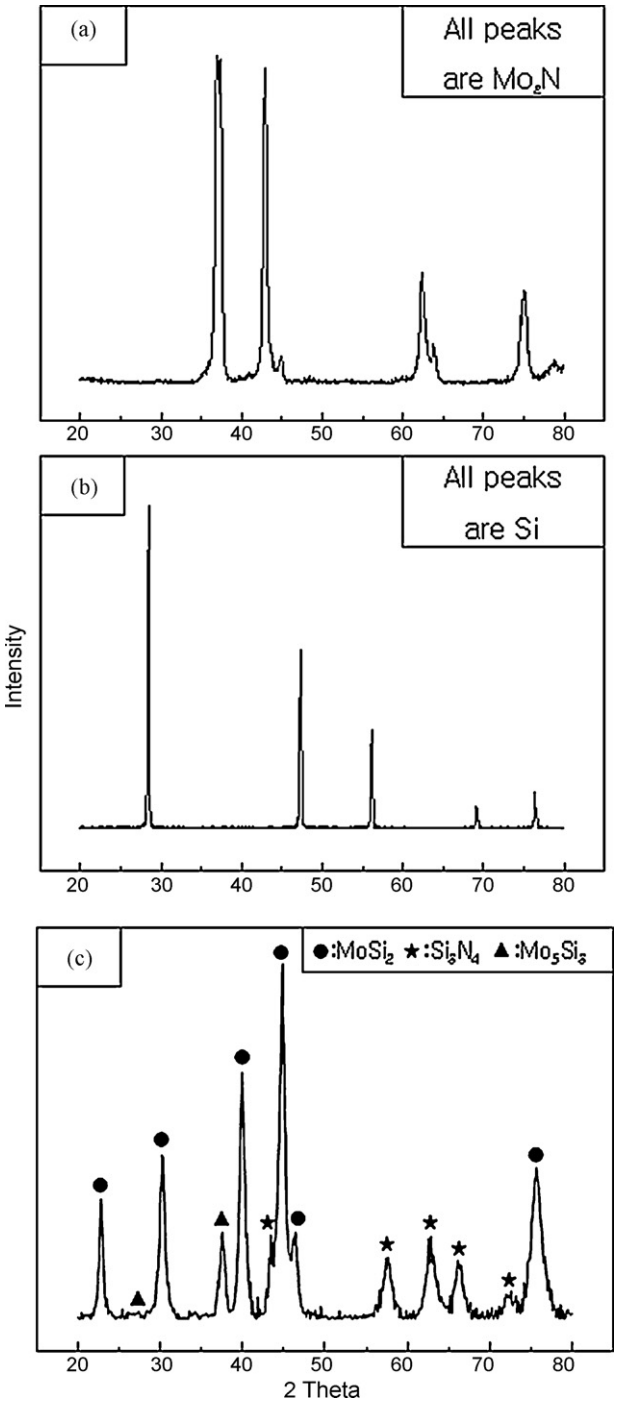

Fig. 1. XRD patterns of the raw materials: (a) Mo_2N, (b) Si and (c) milled $4Mo_2N$+19Si.

Fig. 2 shows the variation in shrinkage displacement and the surface temperature of the graphite die as a function of heating time during densification of $8MoSi_2 + Si_3N_4$. As the pulsed current was applied, thermal expansion was observed up to approximately 1000 °C. Shrinkage displacement then occurred as the temperature was increased further to approximately 1150 °C.

Fig. 3(a) and (b), respectively, show the XRD patterns and FE-SEM image of the etched surface of the samples heated to 1300 °C under pressure of 80 MPa. $MoSi_2$ and Si_3N_4 were detected in the XRD patterns along with a minor phase (Mo_5Si_3). The structure parameters, i.e. the mean grain size of the $MoSi_2$ and Si_3N_4 phases, were obtained from Eq. (1) [25]. The average grain sizes of the

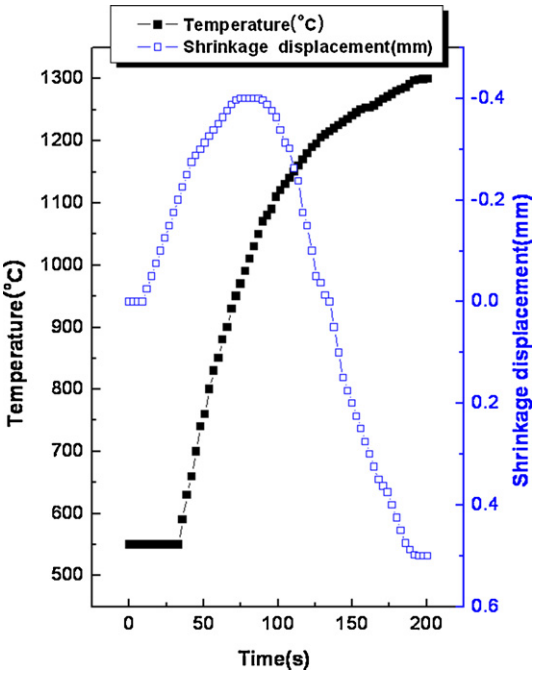

Fig. 2. Changes in temperature and shrinkage displacement with respect to heating time during the densification of $8MoSi_2$–Si_3N_4.

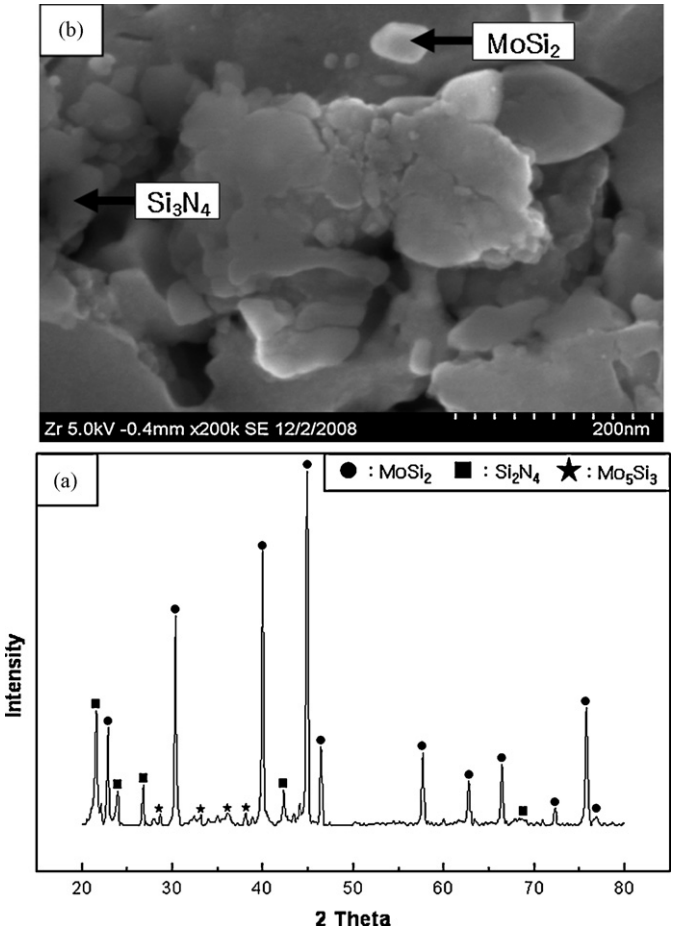

Fig. 3. (a) XRD patterns and (b) FE-SEM image of the $8MoSi_2$–Si_3N_4 composite sintered at 1300 °C.

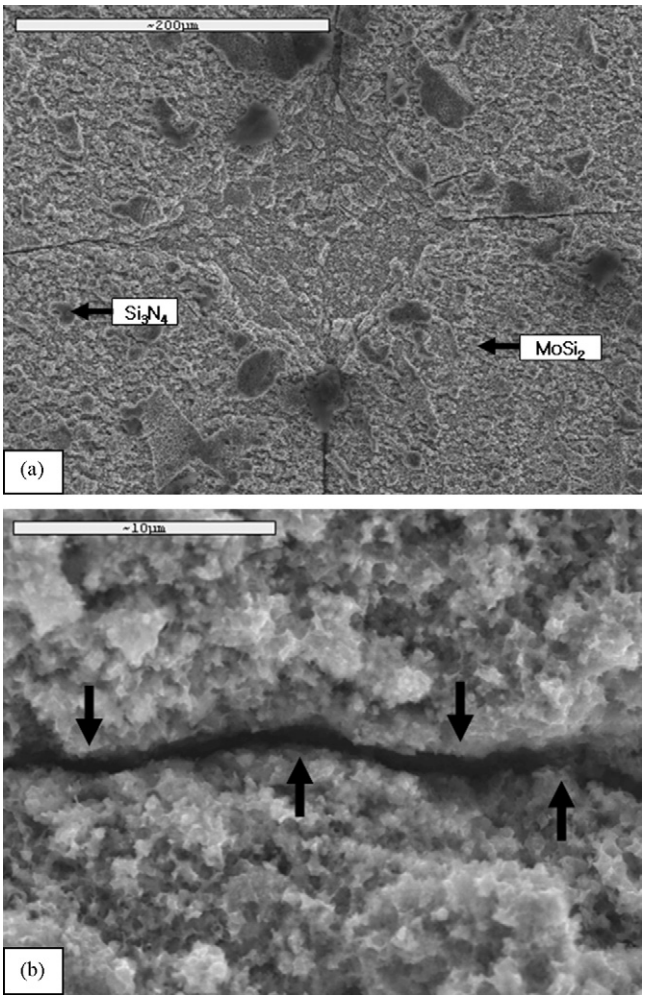

Fig. 4. (a) Vickers hardness indentation and (b) median crack propagation in the $8MoSi_2$–Si_3N_4 composite.

$MoSi_2$ and Si_3N_4 as prepared using the PCAS method, were approximately 100 and 90 nm, respectively. The FE-SEM image also shows the nanophases of the $MoSi_2$–Si_3N_4 composite.

Vickers hardness measurements were made on the polished sections of the $8MoSi_2$–Si_3N_4 composite using a 20 kg load and a 15 s dwell time. The hardness of the $8MoSi_2$–Si_3N_4 composite was calculated to be 1230 kg/mm^2. This value represents an average of five measurements. Indentations with sufficiently large loads produced median cracks around the indent. Fracture toughness values can be determined from the length of these cracks using the following formula reported by Anstis et al. [26]:

$$K_{IC} = 0.016\left(\frac{E}{H}\right)^{1/2} \cdot \frac{P}{C^{3/2}} \quad (3)$$

where E is Young's modulus, H is the indentation hardness, P is the indentation load, and C is the trace length of the crack measured from the center of the indentation. The modulus was estimated by the rule of mixtures for a 0.815 volume fraction of $MoSi_2$ and a 0.185 volume fraction of Si_3N_4 using $E(MoSi_2) = 440$ GPa [27] and $E(Si_3N_4) = 313$ GPa [28]. The toughness obtained from this calculation is 6 ± 0.3 MPa m$^{1/2}$. These fracture toughness and hardness values for the nanostructured $8MoSi_2$–Si_3N_4 composite are higher than those of monolithic $MoSi_2$ (fracture toughness; 2.58 MPa m$^{1/2}$ hardness; 8.7 MPa) [29] owing to the addition of the Si_3N_4 hard phases. As in the case of hardness, toughness value is also the average of five measurements. Fig. 4(a) presents a typical indentation

pattern for the $8MoSi_2$–Si_3N_4 composite. One to three additional cracks were observed to propagate from the indentation corner. Fig. 4(b) shows a view under higher magnification of the indentation median crack in the composite. This shows that the crack propagates deflectively (↑).

Suryanarayana [30] has reported that the density, hardness and fracture toughness of $MoSi_2$–5 wt%Si_3N_4 produced by vacuum hot pressing at 1400 °C and 2000 psi for 1 h are 74.9%, 1010 kg/mm^2, and 2.8 MPa m$^{1/2}$, respectively. Comparing the above study with ours, the relative density and mechanical properties of the $MoSi_2$–Si_3N_4 composite sintered by the PCAS method are higher than those of the composite sintered by hot pressing, even though the sintering temperature for PCAS is lower and the required time shorter. This could be explained in terms of fast temperature rise due to Joule heating, the presence of plasma in pores separating powder particles [31], and the intrinsic contribution of the current to fast mass transport [32–34].

4. Summary

Nanosized $MoSi_2$ and Si_3N_4 powders were synthesized from Mo_2N and Si by high-energy ball milling for 20 h. The $8MoSi_2$–Si_3N_4 composite was consolidated within 3 min by the pulsed current-activated sintering (PCAS) method. The relative density of the composite was 97% at an applied pressure of 80 MPa. The average grain sizes of $MoSi_2$ and Si_3N_4 in the composite prepared by the PCAS method were approximately 100 and 90 nm, respectively. The average hardness and fracture toughness of the nanostructured $8MoSi_2$–Si_3N_4 composite were 1230 kg/mm^2 and 6 MPa m$^{1/2}$, respectively. It can be concluded that the addition of Si_3N_4 and sustenance of nanostructure both enhance the mechanical properties of $MoSi_2$.

Acknowledgement

This study was supported by a National Research Foundation of Korea Grant funded by the Korean Government (2009-0065776).

References

[1] A.K. Bhattacharya, J.J. Petrovic, Mater. Sci. Eng. A 155 (1992) 259–266.
[2] G.J. Fan, M.X. Quan, Z.Q. Hu, J. Eckert, L. Schulz, Scripta Mater. 41 (1999) 1147–1151.
[3] A.K. Vasudevan, J.J. Petrovic, Mater. Sci. Eng. A 155 (1992) 1–17.
[4] R. Mitra, Y.R. Mahajan, N.E. Prasad, W.A. Chiou, C. Ganguly, Key Eng. Mater. 108–110 (1995) 11–15.
[5] J. Milne, Instant Heat, Kinetic Metals Inc., Derby, CT, 1985.
[6] Y.S. Touloukian, R.W. Powell, C.Y. Ho, P.G. Klemens, Thermal Conductivity, IFI/Plenum, New York, 1970.
[7] G. Sauthoff, Intermetallics, VCH Publishers, New York, 1995.
[8] Y. Ohya, M.J. Hoffmann, G. Petzow, J. Mater. Sci. Lett. 12 (1993) 149–152.
[9] J. Qian, L.L. Daemen, Y. Zhao, Diam. Relat. Mater. 14 (2005) 1669–1672.
[10] Q. Hu, P. Luo, Y. Yan, J. Alloys Compd. 468 (2009) 136–142.
[11] Y. Ohya, M.J. Hoffmann, G. Petzow, J. Am. Ceram. Soc. 75 (1992) 2479–2483.
[12] S.K. Bhaumik, C. Divakar, A.K. Singh, G.S. Upadhyaya, J. Mater. Sci. Eng. A 279 (2000) 275–281.
[13] D.K. Jang, R. Abbaschian, Kor. J. Mater. Res. 9 (1999) 92–98.
[14] D.Y. Oh, H.C. Kim, J.K. Yoon, I.J. Shon, J. Alloys Compd. 395 (2005) 174–180.
[15] J.K. Yoon, G.H. Kim, J.H. Han, I.J. Shon, J.M. Doh, K.T. Hong, Surf. Coat. Technol. 200 (2005) 2537–2546.
[16] O.K. Varghese, J. Latempa, Nano Lett. 9 (2009) 731–735.
[17] D. Donadio, G. Galli, Nano Lett. 10 (2010) 847–851.
[18] M.G. Lines, J. Alloys Compd. 449 (2008) 242–245.
[19] C. Menapace, I. Lonardelli, M. Tait, A. Molinari, Mater. Sci. Eng. A 517 (2009) 1–7.
[20] W. Dressler, R. Riedel, Progress, Int. J. Refract. Met. Hard Mater. 15 (1997) 13–47.
[21] S.P. Taguchi, S. Ribeiro, J. Mater. Proc. Technol. 147 (2004) 336–342.
[22] T. Murakami, S. Sasaki, K. Ichikawa, A. Kitahara, Intermetallics 9 (2001) 621–628.
[23] I.J. Shon, D.K. Kim, K.T. Lee, K.S. Nam, Met. Mater. Int. 14 (2008) 593–598.
[24] S.K. Bae, I.J. Shon, J.M. Doh, J.K. Yoon, I.Y. Ko, Scripta Mater. 58 (2008) 425–428.
[25] C. Suryanarayana, M. Grant Norton, X-ray Diffraction: A Practical Approach, Plenum Press, New York, 1998.
[26] G.R. Anstis, P. Chantikul, B.R. Lawn, D.B. Marshall, J. Am. Ceram. Soc. 64 (1981) 533–538.
[27] I.J. Shon, Z.A. Minir, K. Yamazaki, K. Shoda, J. Am. Ceram. Soc. 79 (1996) 1875–1880.
[28] M. Lugovy, V. Slyunyayev, V. Subbotin, N. Orlovskaya, G. Gogotsi, Compos. Sci. Technol. 64 (2004) 1947–1957.
[29] K. Robert, Wade, J. Am. Ceram. Soc. 75 (1992) 1682–1684.
[30] C. Suryanarayana, Mater. Sci. Eng. A 479 (2008) 23–30.
[31] Z. Shen, M. Johnsson, Z. Zhao, M. Nygren, J. Am. Ceram. Soc. 85 (2002) 1921–1927.
[32] J.E. Garay, U. Anselmi-Tamburini, Z.A. Munir, S.C. Glade, P. Asoka-Kumar, Appl. Phys. Lett. 85 (2004) 573–575.
[33] J.R. Friedman, J.E. Garay, U. Anselmi-Tamburini, Z.A. Munir, Intermetallics 12 (2004) 589–597.
[34] J.E. Garay, U. Anselmi-Tamburini, Z.A. Munir, Acta Mater. 51 (2003) 4487–4495.